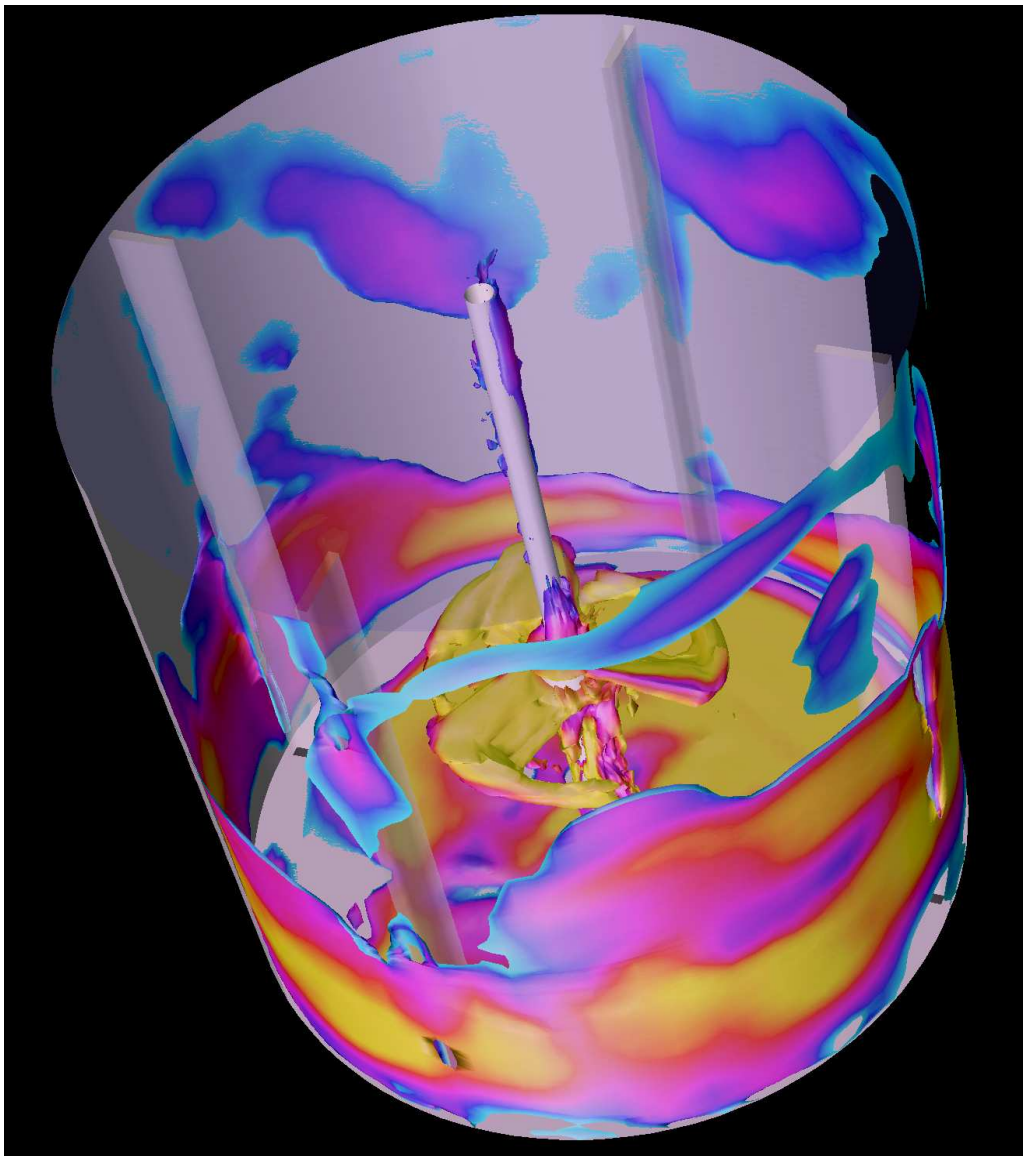


Modeling Of Turbulence In Stirred Vessels Using Large Eddy Simulation

André Bakker

Fluent, Inc., 10 Cavendish Court, Lebanon NH 03766, USA
Phone: 603-643-2600; fax: 603-643-3967; e-mail: ab@fluent.com.



Keywords: Large Eddy Simulation, LES, Mixing, Turbulence.
Published in the Online CFM Book at <http://www.bakker.org/cfm>
(c) 2003 André Bakker

ABSTRACT

The application of large eddy simulation (LES) to the prediction of large-scale chaotic structures in stirred tanks is investigated. Flow regimes representing typical stirrer configurations were assessed: a single radial pumping impeller and a single axial pumping pitched blade turbine. The turbulent flow field in each configuration was calculated using LES turbulence models. The impellers were modeled using the sliding mesh model. The predicted flow patterns compared well with digital particle image velocimetry data reported in the literature, and exhibited the long time scale instabilities seen in the experiments. The results of these studies open the way to a renewed interpretation of many previously unexplained hydrodynamic phenomena that are observed in stirred vessels.

1. INTRODUCTION

Prediction of mixing of multi-component fluids is important in many chemical process applications. Although laminar mixing is a complicated process per se, there is a far greater challenge in predicting the mixing in turbulent flows because of the intrinsic, chaotic nature of turbulent flows. In turbulent flows, large-scale eddies with coherent structures are mainly responsible for the mixing of passive scalars. The large-scale eddies embody themselves in the form of identifiable and organized distributions of vorticity.

Recent experimental work suggests that large-scale, time-dependent structures, with periods much longer than the time of an impeller revolution, are involved in many of the fundamental hydrodynamic processes in stirred vessels. For example, local velocity data histograms may be bi-modal or tri-modal, even though they are usually analyzed as having only one mode in most laser-Doppler experiments (Bakker and Van den Akker, 1994a). The gas holdup distribution may be asymmetric and oscillating (Bakker and Van den Akker, 1994b). In solids suspension processes, solids can be swept from one side of the vessel to the other in a relatively slow oscillating pattern, even in dilute suspensions. Digital particle image velocimetry experiments have shown that large-scale asymmetries with periods up to several minutes exist in stirred vessels equipped with axial flow impellers (Myers et al. 1997).

In this study, the application of LES to the prediction of these large-scale chaotic structures in stirred tanks is investigated. Several flow regimes representing typical stirrer configurations were assessed: a single radial pumping impeller, a single axial pumping pitched blade turbine, a single high-efficiency impeller, and a dual impeller combination. Because of space constraints, however, only the results for the former two systems will be discussed in detail in this article. Results include the blending of a tracer. Previous LES work reported in the literature considered radial flow impellers only (Eggels, 1996. Derksen and Van den Akker, 1999) and did not include blending studies. The impeller rotation was modeled using a sliding mesh model on unstructured grids (Mathur, 1994. Bakker et al. 1997). The theory behind LES, the model, and the results will be discussed.

This chapter is based on a paper presented by Bakker et al. (2000) at the 10th European Mixing Conference. It contains material from both the proceedings, and unpublished material from the oral presentation at this conference.

2. THEORETICAL

2.1 The LES Model

The numerical modeling of these complicated mixing processes is a daunting task. Direct numerical simulation (DNS) provides the most exact approach in which the mechanism involved in turbulent mixing can be accurately represented. DNS requires resolving the smallest eddies which makes the approach prohibitively expensive even with the most powerful computers of the present day, and foreseeable future as well. On the other hand, the popular approaches based on the Reynolds-averaged Navier-Stokes (RANS) equations amount to averaging out the large eddies that are mainly responsible for mixing. One is left to model the effects of large eddies by relying on empirical data and phenomenological reasoning and hypotheses.

Recently, the large eddy simulation (LES) approach has been used as an intermediate method between the extremes of DNS and RANS. The premise underlying LES is that any turbulent flow consists of eddies, and involves a wide spectrum of scale. In LES, large eddies are resolved directly, and small eddies are modeled. The rationale behind LES can be summarized as follows. Momentum, mass, energy, and other passive scalars are transferred mostly by large eddies. Large eddies are more dependent on the geometries and boundary conditions of the flow involved, and are highly anisotropic. Small eddies are less dependent on the geometry, and tend to be more isotropic, and consequently are more universal. The chance of finding an universal model is much higher when only small eddies are modeled. In the LES approach, the governing equations are obtained by spatially filtering the Navier-Stokes equations. The large turbulent scales are computed explicitly, while the small scales are modeled using one of a number of available subgrid scale (SGS) models. The SGS models describe interactions between the resolved and unresolved scales. The LES approach is more general than the RANS approach, and avoids the RANS dependence on boundary conditions for the large scale eddies. Like DNS, the LES approach gives a three-dimensional, time dependent solution. The required computational resources for LES are between those of the DNS and RANS approaches. The LES model can be used at much higher Reynolds numbers than DNS because the computational effort is independent of the Reynolds number if the small scales obey the inertial range spectrum and the near wall effects are not important.

2.2 Governing Equations

The governing equations for LES are obtained by spatially filtering over small scales. Filtering eliminates the eddies whose scales are smaller than the filter width. In the current study, a top-hat filter of filter width to grid size ratio of two is used. Explicit filtering is not used. With this filter, differentiation and filtering operations commute only on uniform grids. The importance of commutation errors on non-uniform grids is a topic of current research. In the present work, it is assumed that the commutation error is a part of the error in the subgrid models. Applying the filtering operation to the momentum equation, we obtain:

$$\frac{\partial \bar{\rho} \tilde{u}_i}{\partial t} + \frac{\partial \bar{\rho} \tilde{u}_i \tilde{u}_j}{\partial x_j} = -\frac{\partial \bar{p}}{\partial x_i} + \frac{\partial \bar{\tau}_{ij}}{\partial x_j} + \frac{\partial \sigma_{ij}}{\partial x_j} \quad (1)$$

where $\bar{\tau}_{ij}$ is the filtered (subgrid scale) stress tensor. In the filtered equations, the terms represented by σ_{ij} , called SGS stresses/fluxes, are of the form:

$$\sigma_{ij} = -(\overline{\rho u_i u_j} - \bar{\rho} \tilde{u}_i \tilde{u}_j) \quad (2)$$

These SGS stresses/fluxes are unknown, and need to be modeled. Smagorinsky (1963) and Lilly (1966) developed the most basic subgrid scale model. In this model, the turbulent viscosity is modeled by:

$$\mu_t = \rho L_s^2 |\bar{S}| \quad (3)$$

where L_s is the mixing length for subgrid scales, and $|\bar{S}| = \sqrt{2\bar{S}_{ij}\bar{S}_{ij}}$. The mixing length, L_s , is computed in FLUENT as $\mu L_s = \min(\kappa d, C_s V^{1/3})$ where κ and C_s are constants, d is the distance to the closest wall, and V is the volume of the cell.

Yakhot et al. (1986) have obtained an RNG subgrid scale stress model by performing recursive elimination of infinitesimal bands of small scales. In the RNG SGS model, subgrid fluxes in the momentum equation are represented by:

$$\sigma_{ij} - \frac{1}{3}\sigma_{kk}\delta_{ij} = 2\mu_{sgs}\tilde{S}_{ij} \quad (4)$$

This model differs from the Smagorinsky model in the way subgrid viscosity is calculated. In the RNG subgrid model, the effective viscosity, $\mu_{eff} = \mu + \mu_t$, is given by:

$$\mu_{eff} = \mu \left[1 + H\left(\frac{\mu_{sgs}^2 \mu_{eff}}{\mu^3} - C\right) \right]^{1/3} \quad (5)$$

where $\mu_{sgs} = \bar{\rho}(C_{rng}\Delta)^2(2\bar{S}_{ij}\bar{S}_{ij})^{1/2}$ and $H(x)$ is the Heaviside ramp function. The coefficients, $C_s = 0.157$ and $C=100$ are obtained from the theory.

In highly turbulent regions, the filtering operation results in very high subgrid viscosity compared to the molecular viscosity, $\mu_{sgs} \gg \mu$ and $\mu_{eff} \cong \mu_{sgs}$. In this limit, the RNG theory based subgrid scale model returns to the Smagorinsky model with a different model constant. In weakly turbulent regions, the argument of the Heaviside function is negative, and the effective viscosity is equal to the molecular viscosity. The RNG SGS model in this limit correctly yields zero SGS viscosity in low Reynolds number flows without any ad-hoc modifications.

2.3 Numerical Method

The numerical simulations are conducted using FLUENT. A detailed discussion of the numerical method and several validation studies of this code are given by Murthy and Mathur (1998). In this code, the domain is discretized into arbitrary unstructured polyhedra. The discretized form of the governing equations for each cell is obtained such that the conservation principles are obeyed on each polyhedron. In FLUENT, the linear equations are solved using an algebraic multigrid procedure. The results presented in this

paper are obtained using central differencing for spatial discretization of the momentum equations, and time-advancement via a second-order accurate implicit scheme. The transient impeller motion was modeled using the sliding mesh model for unstructured grids (Mathur, 1994).

3. MODEL DESCRIPTION

The modeling results of the transient, turbulent hydrodynamics will be reported for four configurations. The first was a 45° pitched-blade turbine (PBT) configuration consisting of a cylindrical, flat-bottomed tank of internal diameter, $T = 292\text{mm}$, with four full-length baffles of width $T/12$. The free surface was at a height, $H=T$. The PBT had four blades, with a diameter $D=0.35T$, a blade width $W=0.20D$, and a blade thickness of 1 mm. The impeller center was positioned at a distance $C=0.46T$ off the tank bottom. The impeller was mounted on a 10mm diameter shaft rotating at 60rpm. This geometry was studied experimentally by Myers et al. (1997). The computational grid was defined by 527,000 unstructured, non-uniformly distributed, hexahedral cells. Approximately 180 seconds of actual time were simulated. All simulations were initiated from a zero-velocity flow field.

The Rushton turbine configuration consists of a cylindrical, flat-bottomed tank of internal diameter, $T = 202\text{mm}$, with four full-length baffles of width 22mm. The free surface was at a height, $H=T$. The impeller had a diameter $D=T/3$, a blade width $W=0.20D$ and a blade thickness of one mm. The impeller center was positioned at a distance $C=T/3$ off the tank bottom. The impeller was mounted on a 5mm diameter shaft rotating at 290rpm. The computational grid was defined by 763,000 unstructured, non-uniformly-distributed, hexahedral cells. Approximately 3 seconds of actual time were simulated. Implicit time steps of 0.01 to 0.05 seconds were used.

A system with a single three blade high-efficiency impeller was also simulated. The simulations were performed for a flat bottom vessel with four baffles. The vessel diameter was $T=0.292\text{m}$. The liquid level was equal to the tank diameter, $Z/T=1$. The liquid was water. The impeller was a Chemineer HE-3 with a D/T of 0.39 and an off bottom clearance of $C/T=0.33$. The impeller speed was 60 RPM and the impeller Reynolds number was approximately $1.3E4$. This was the same system as studied experimentally by Myers et al. (1997).

Furthermore, a vessel equipped with four A310 impellers was studied. The vessel diameter was 0.232 m. The liquid level was 0.944 m ($Z/T=4$). The impeller diameter was 0.097 m ($D/T=0.42$) for all impellers. The distance between the impellers was 0.236 m. The lower impeller was located 0.118 m above the vessel bottom. The liquid was water. The vessel was closed with a flat lid on top. The vessel is equipped with four baffles with $W/T=0.1$. The baffles were attached to the wall. This geometry is similar to an experimental system being studied at the University of Bologna (Magelli and Montante, 2002). Finally, a the flow field in a typical glass lined vessel equipped with a retreat blade impeller was evaluated.

4. RESULTS

4.1 Flow Field Results for the PBT

Figure 1 shows vector plots after 162, 166, 170, and 174 seconds respectively for the simulations with the pitched blade turbine. These vector plots show the unsteadiness in the flowfield. Figure 1a shows a relatively symmetric axial flow pattern. Figure 1b shows an asymmetric flow pattern, with the flow on the left side of the vessel being axial, and the jet coming from the impeller attaching to the vessel bottom. On the right side of the vessel, the jet coming from the impeller bends radially and attaches to the vessel wall. Figure 1c shows a flow pattern where the jet coming from the impeller attaches to the vessel wall on both sides and a secondary circulation loop has formed near the vessel bottom. Figure 1d shows a relatively symmetrical flow pattern where the axial jet from the impeller attaches to the vessel bottom.

Qualitatively, these results compare strikingly well with the digital particle image velocimetry data reported by Myers et al. (1997). Their experimental data also showed the existence of these unsteady, asymmetric flow patterns.

Note that these flow pattern oscillations have a time scale that is much longer than the time scale associated with the impeller blade passage frequency. Figure 2 shows the simulated flow patterns at three instances in time, spaced apart by half a blade passage period, or 0.125s. The overall flow pattern, which is asymmetric, does not change during that time. This also agrees with the experimental data reported by Myers et al. (1997).

4.2 Time Series Results for the PBT

Figure 3 shows time series of the axial velocity in four locations. A Cartesian reference frame is used with the origin being on the axis at the liquid surface, and x being the downward axial direction. Significant fluctuations can be observed, with the axial velocity periodically changing direction in certain locations. These time series also show that the period of the fluctuations is not constant. Higher frequency variations are observed in locations (a) and (b), which are located just below the impeller blade tip, than in locations (c), close to the vessel bottom, and (d), which is close to the liquid surface. More advanced time series analysis, including spectral analysis, will be a topic of future research.

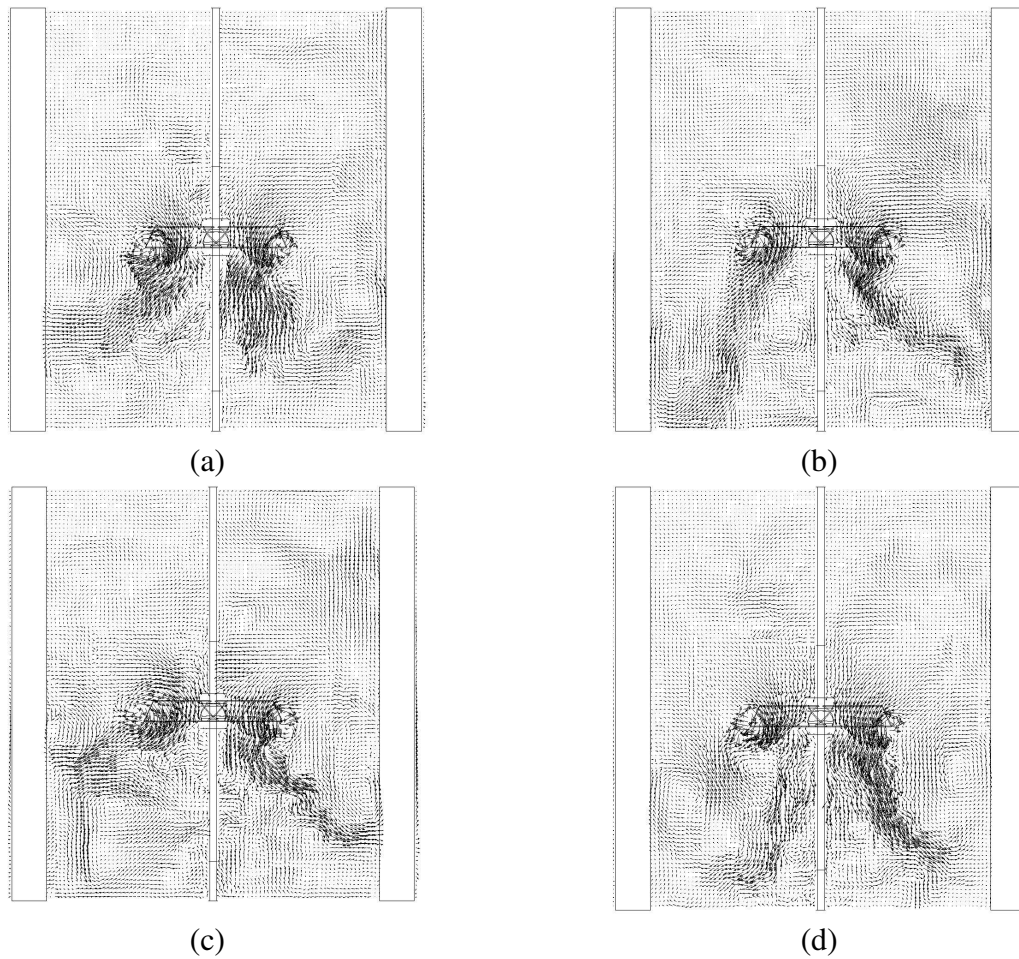


Figure 1 The pitched blade turbine flow pattern after 162, 166, 170, and 174 seconds.

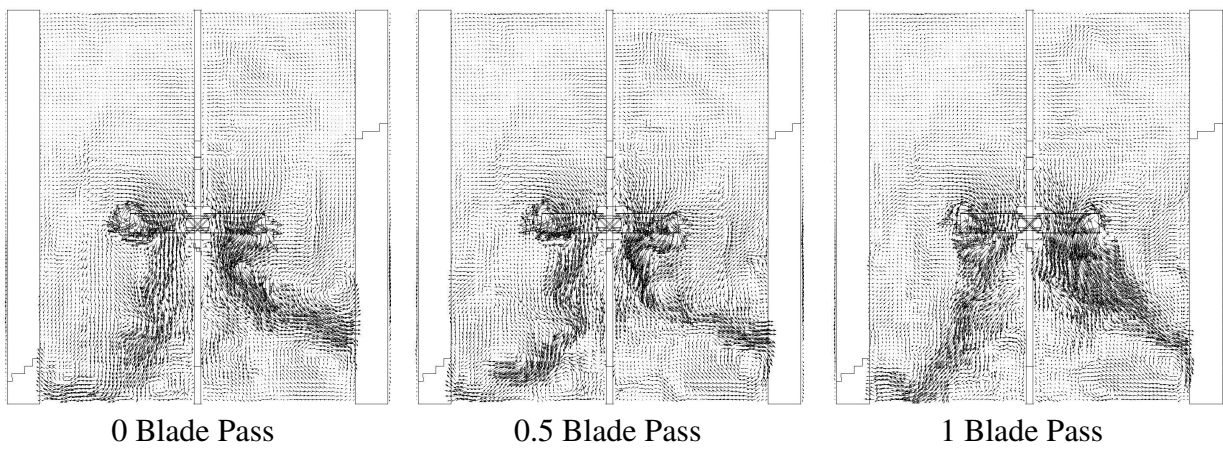


Figure 2 Instantaneous velocity fields of the PBT taken during blade passage.

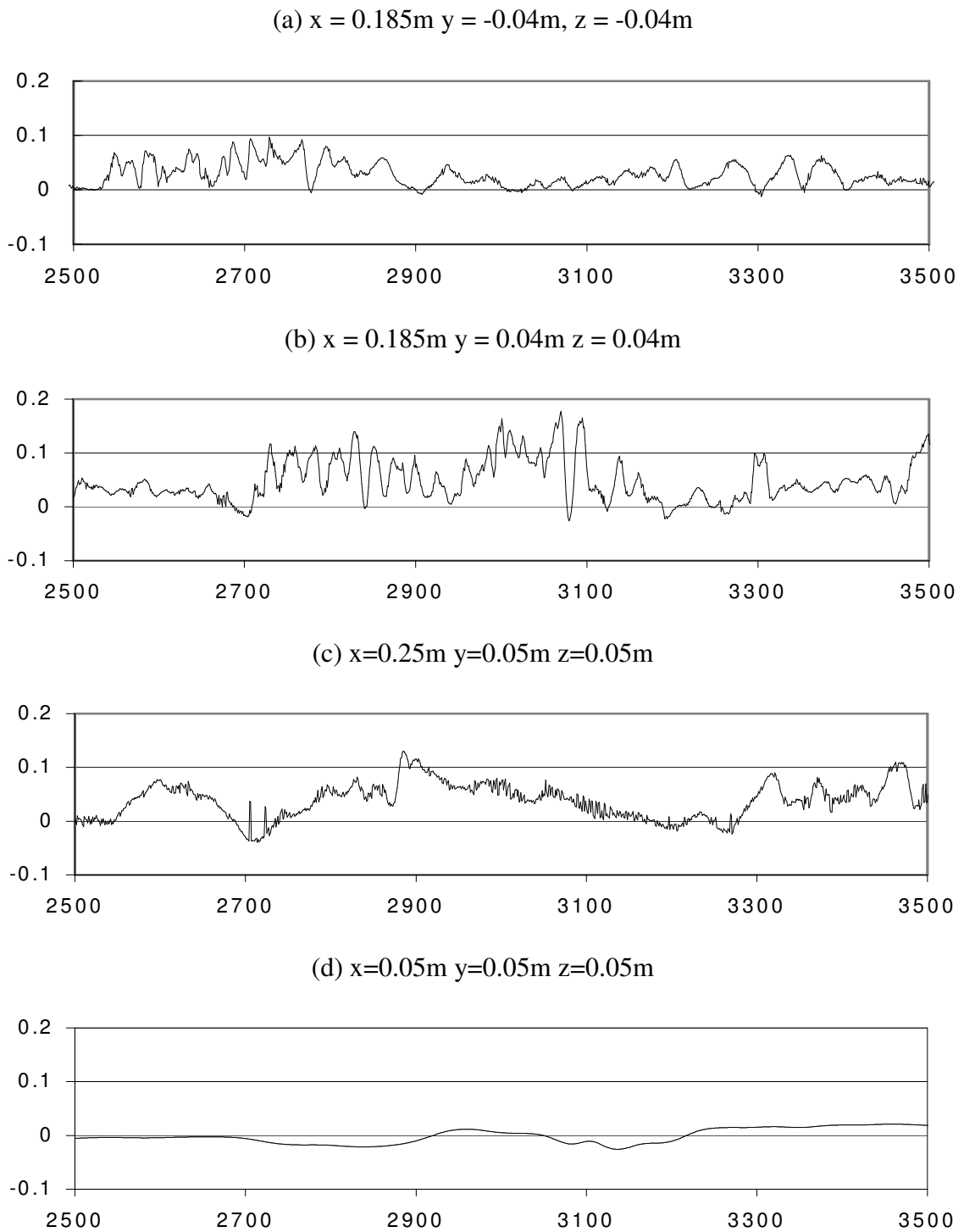


Figure 3 Time series plots of axial velocity for the PBT from 168.13306 (2500 time steps) to 178.12756s (3500 time steps) after start-up from a zero-velocity field.

4.3 Blending Results for the PBT

Figure 4 shows the blending of a tracer injected just above the tip of the PBT. The results show that the tracer does not disperse symmetrically, indicating that such simulations need to be performed on full 360-degree grids, instead of periodic 90-degree sectors.



Figure 4 Blending of a tracer in the unsteady flow field created by a PBT.

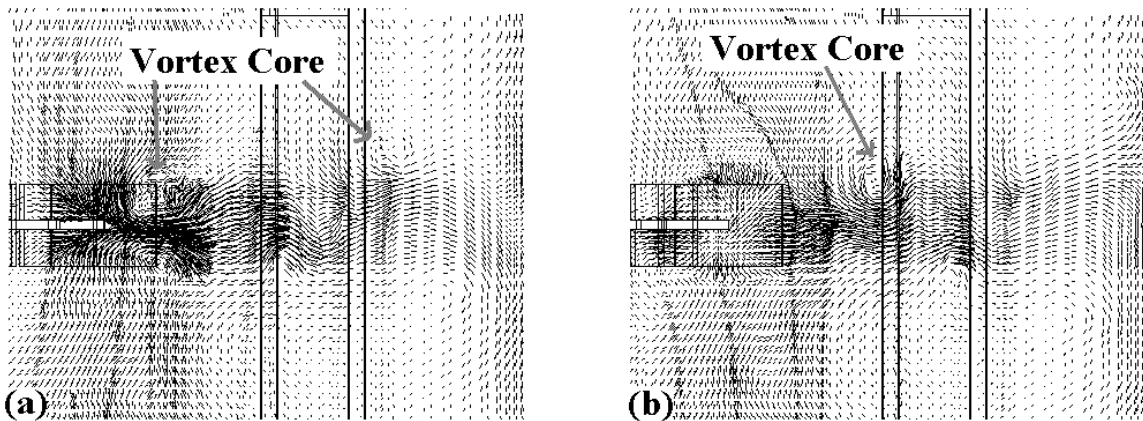


Figure 5 The unsteady flow created by a Rushton turbine.

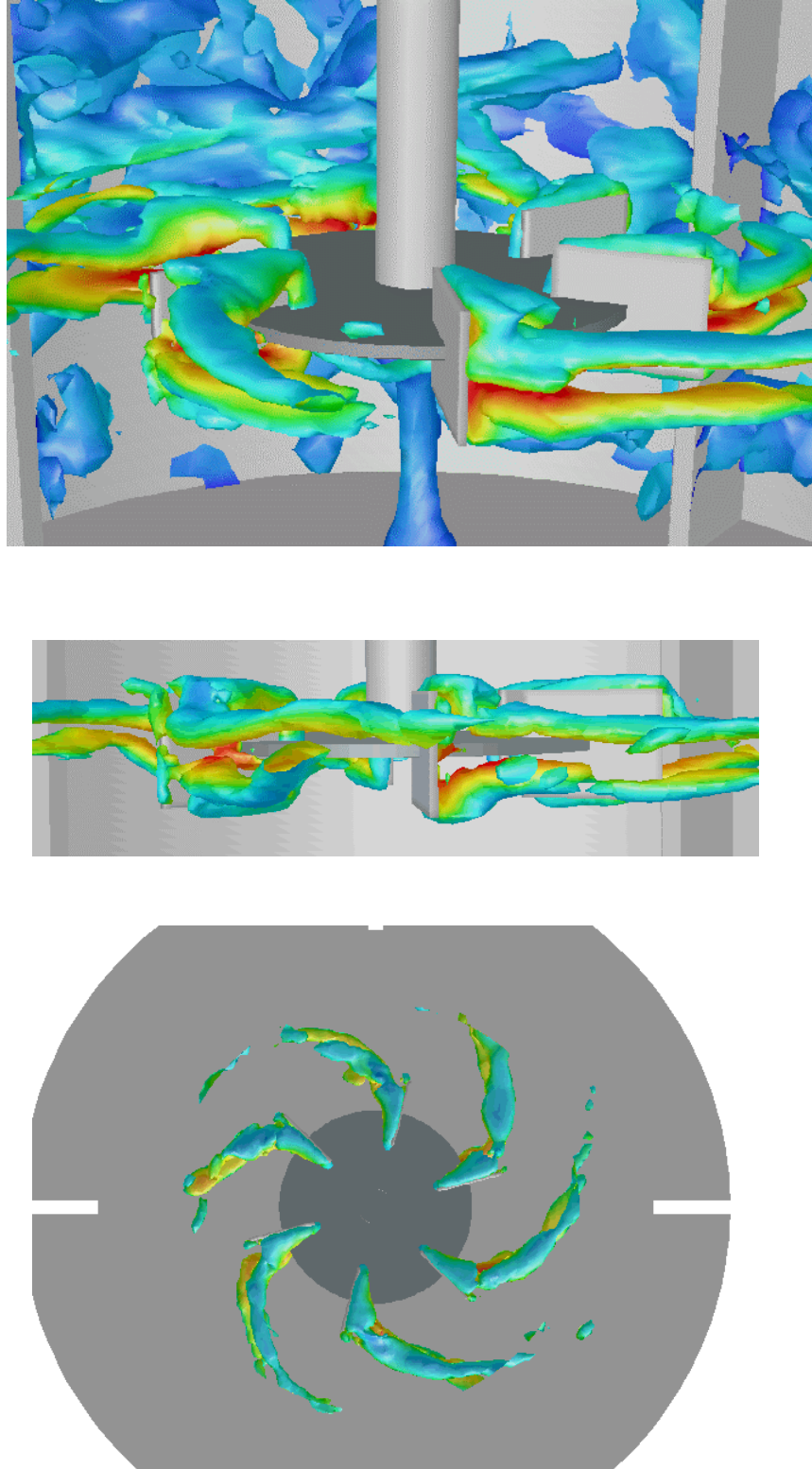


Figure 6 The vortices created behind the blades of a Rushton turbine, at one instant in time. The vortices are visualized by means of an iso-surface of vorticity magnitude (550 s^{-1}), colored by velocity magnitude.

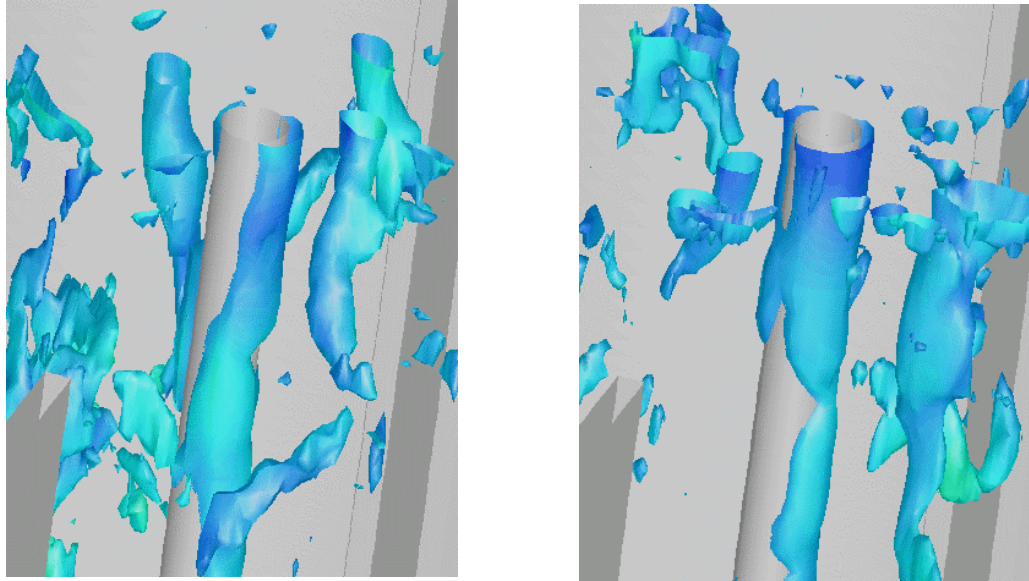


Figure 7 The vortices near the shaft at two different instances in time. The vortices are visualized by means of an iso-surface of vorticity magnitude (80 s^{-1}), colored by velocity magnitude.

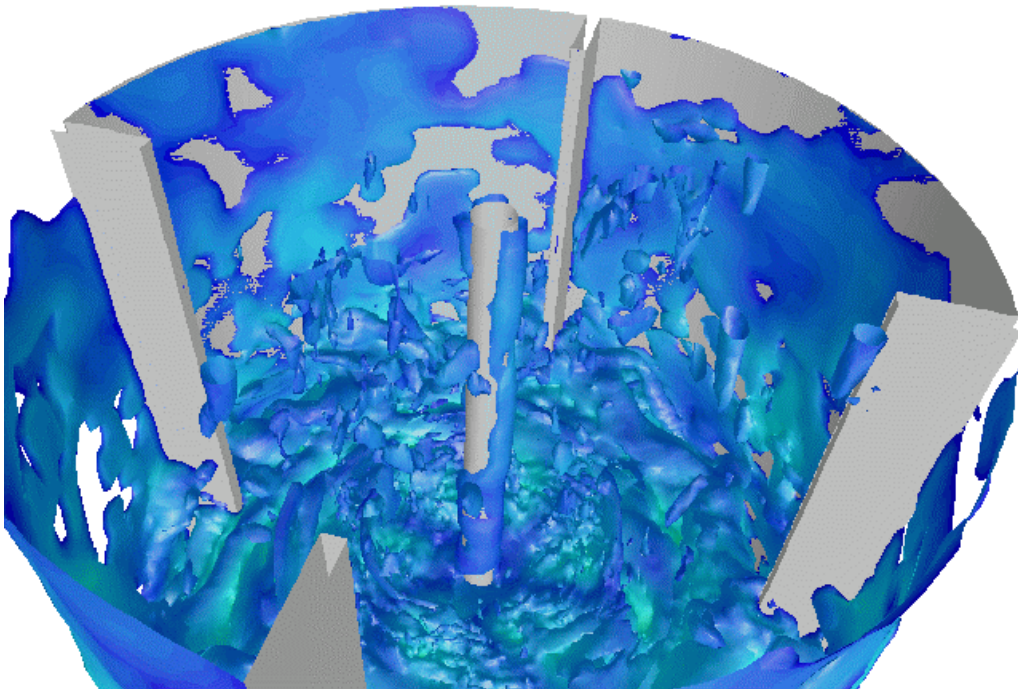


Figure 8 The turbulent flow field at one instant in time, visualized by means of an iso-surface of vorticity magnitude (80 s^{-1}) colored by velocity magnitude.

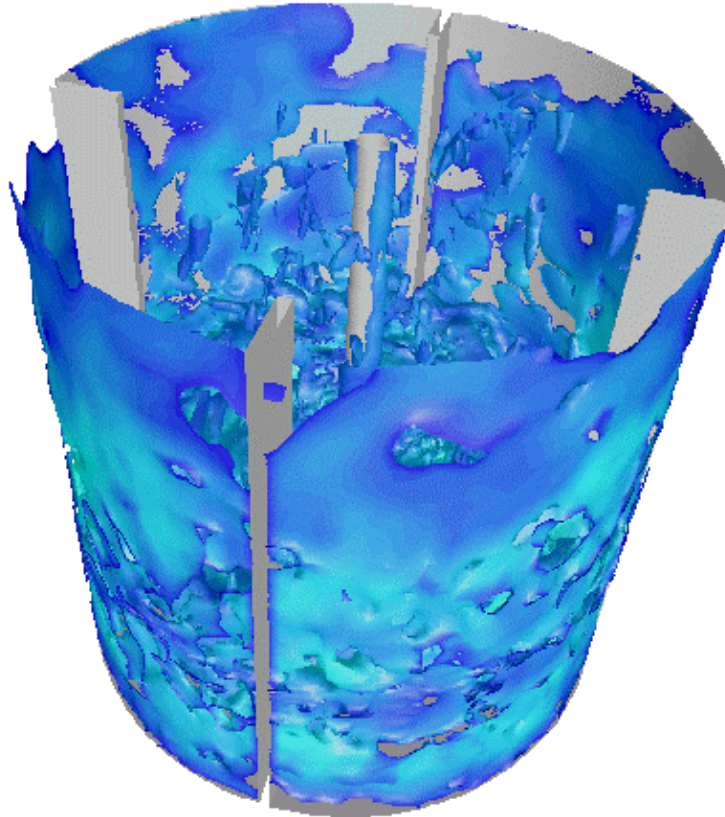


Figure 9 The turbulent flow field in the vessel at one instant in time, visualized by means of an iso-surface of vorticity-magnitude (80 s^{-1}) colored by velocity magnitude.

4.4 Instantaneous Flow Field for the Rushton Turbine

Figure 5 shows the unsteady flow field in the outflow of the Rushton turbine, at two instances in time separated by 0.024s, which corresponds to 0.7 of a blade passage period. Figure 5a shows the trailing vortex forming just behind the impeller blade on the left. The vortex core indicated on the right in Figure 5a is the core of the trailing vortex behind the previous blade. Figure 5b shows how the vortex core coming from the blade has moved radially outwards. These results qualitatively agree with the results reported by Eggels (1996) and Derksen and Van den Akker (1999).

Figures 6 through 9 show the vortices behind the impeller blade, vortices at the liquid surface, and overall views of the turbulent flow field at various instances in time, for the Rushton turbine. It should be noted that the flow field is unsteady, and that these images show snapshots of the flow field only. For example, the vortices near the shaft are highly unsteady, and vortices form, move, and decay in an unsteady fashion.

4.5 Instantaneous Flow Field for the HE-3 Impeller

Figure 10 shows an instantaneous flow field result for the HE-3 impeller. The flow is shown by means of so-called oilflow lines at the liquid surface. Oilflow lines are pathlines that are constrained to a given surface. Figure 11 shows the oilflow lines at the vessel wall at the same instant in time. The oilflow lines are colored by velocity magnitude, with red denoting a high velocity and blue indicating a low velocity. The complex turbulent structures that form within the vessel are clearly visible. Vortices are visible at the liquid surface.

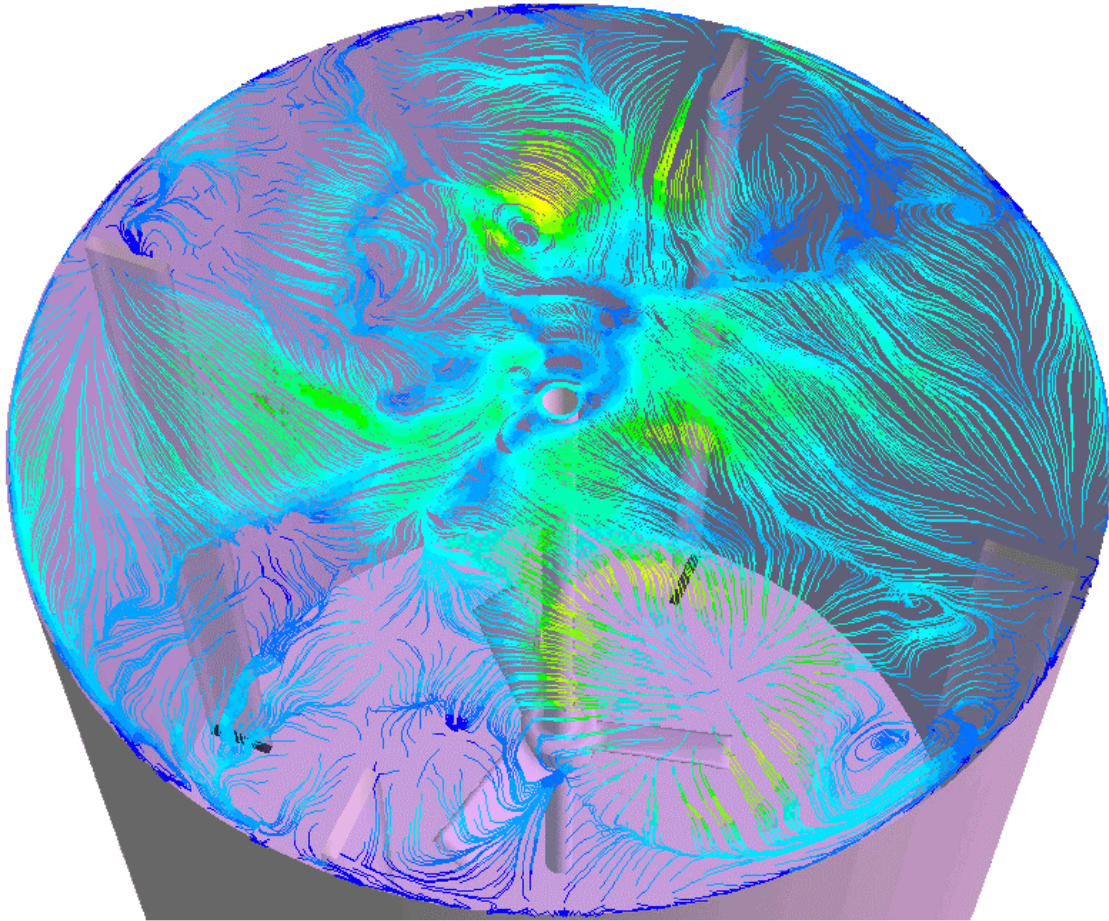


Figure 10. Oilflow lines at the liquid surface for an HE-3 impeller.

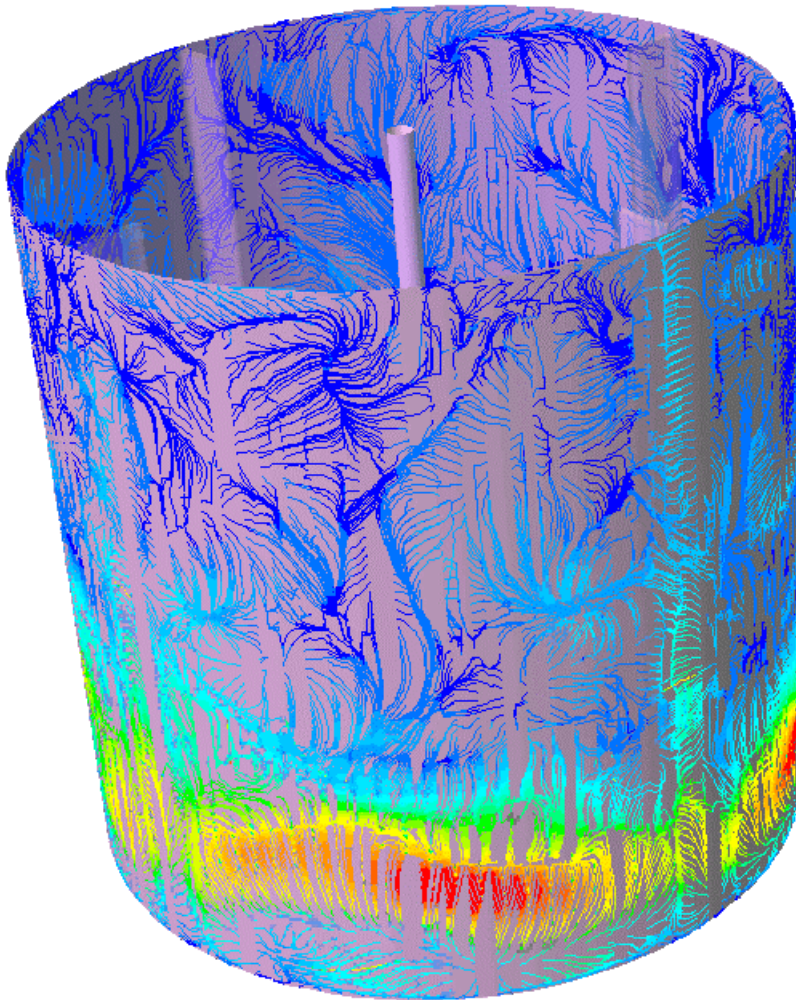


Figure 11. Oilflow lines at the vessel wall for an HE-3 impeller.

4.5 Instantaneous Flow Field for the Multiple A310 Impeller System

Figure 12 shows instantaneous flow field results for the multiple A310 impeller system. The flow is shown by means of contour plots of velocity magnitude. The different outflow pattern for each of the four impellers is clearly visible. Obviously, these flow patterns are unstable, with the flow between the impellers periodically separating and reattaching.

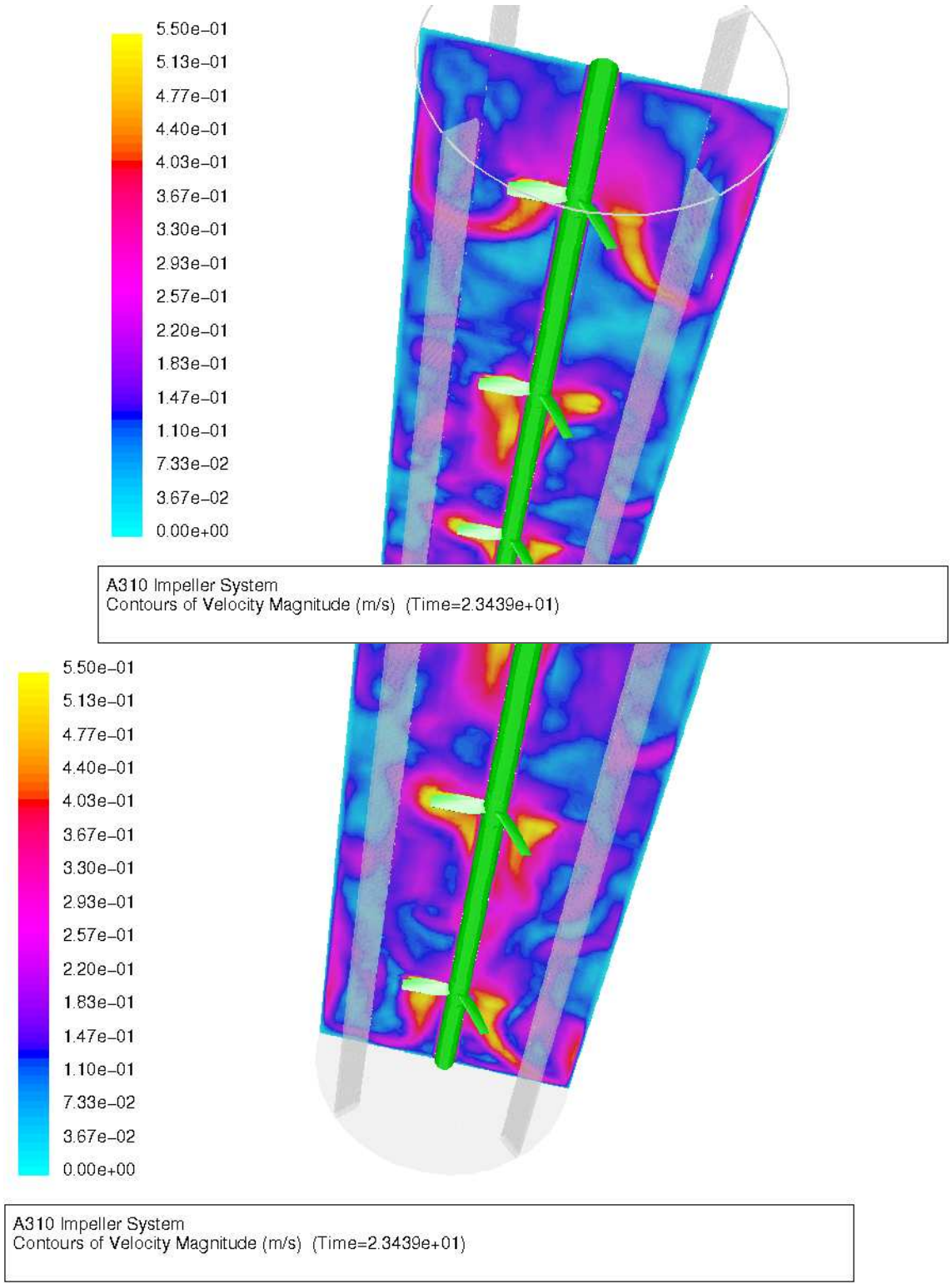


Figure 12 Instantaneous flow field result for the multiple A310 system.

5. GLASS LINED MIXING EQUIPMENT

Figure 14 shows the geometry of a typical glass lined mixing vessel. Glass lined equipment is typically used for applications that involve highly corrosive materials. The glass coating is inert with respect to the chemical reaction, thus protecting the metal from the corrosive chemicals. The geometry of impellers, baffles, and vessels in glass lined systems is restricted by the fact that there can be no sharp edges, to which the glass would not adhere, and by the fact that baffles have to be suspended from flanges in the top head. They can not be welded or bolted to the vessel as is common in other applications. Thus the geometry of glass lined mixing systems is typically very different from so-called “alloy equipment.” Figure 15 shows droplet dispersion in a glass lined vessel equipped with a retreat curve impeller. The droplets are injected from the dip tube and dispersed from there. The center plane is colored by liquid velocity magnitude. Figure 16 shows the flow field at the liquid surface of this vessel as shown by so-called oilflow lines. The color denotes the local liquid velocity.

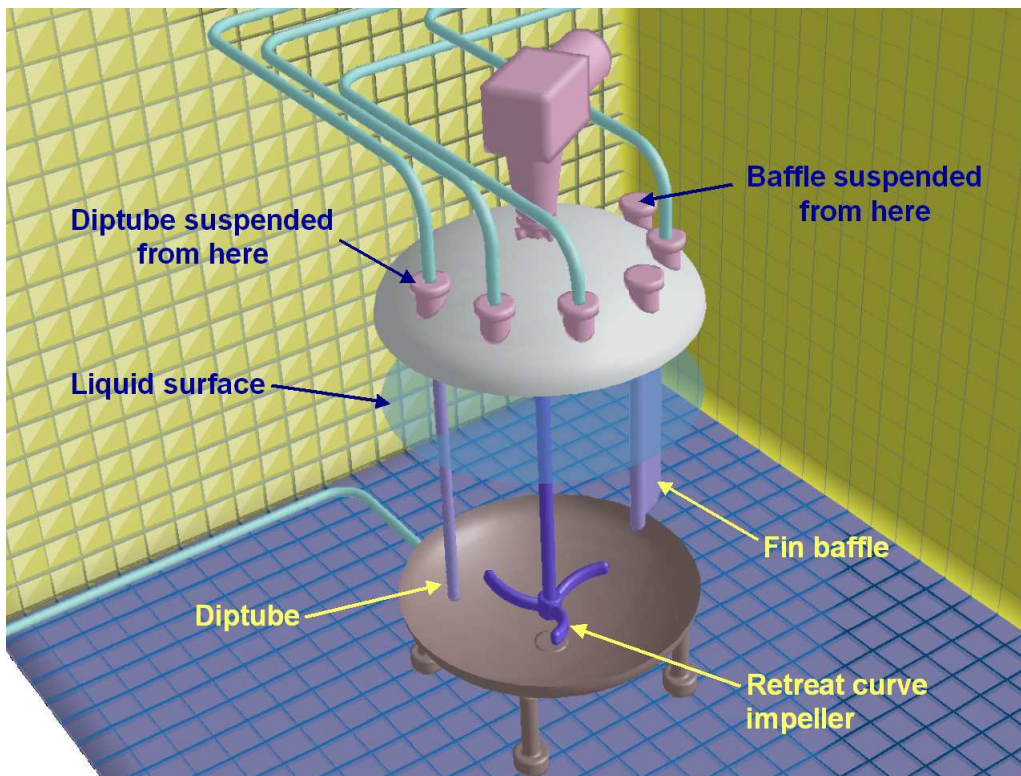


Figure 14 Geometry of a typical glass lined mixing vessel.

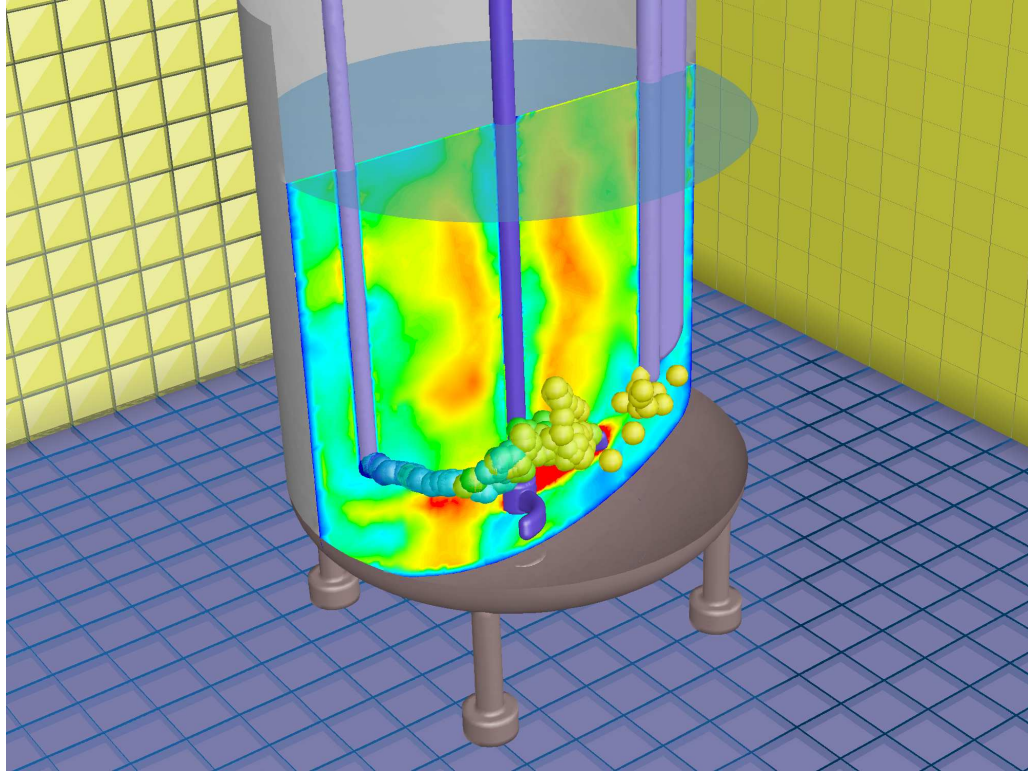


Figure 15 Droplet dispersion in a glass lined vessel equipped with a retreat curve impeller. The droplets are injected from the dip tube and dispersed from there. The center plane is colored by liquid velocity magnitude.

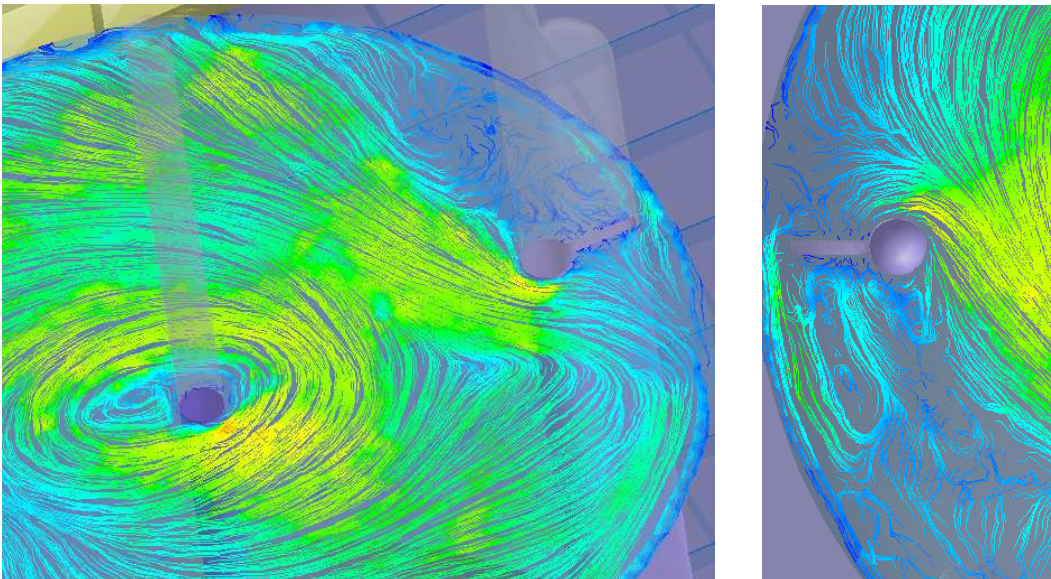


Figure 16 The flow field at the liquid surface of this vessel as shown by so-called oilflow lines. The color denotes the local liquid velocity.

6. CONCLUSIONS

In this study, the application of large eddy simulation (LES) to the prediction of large-scale chaotic structures in stirred tanks was investigated. Flow regimes representing typical stirrer configurations were assessed. The predicted flow patterns for the PBT compared well with digital particle image velocimetry data reported in the literature, and exhibited the long time scale instabilities seen in the experiments. The results for the Rushton turbine compared well with LES simulations reported previously. The results of these studies open the way to a renewed interpretation of many previously unexplained hydrodynamic phenomena that are observed in stirred vessels, such as the time dependent settling of solids in dilute suspensions, bi-modal and tri-modal velocity histograms observed in laser-Doppler experiments, large variations in measured blend times in seemingly identical experiments, and possibly even the observed asymmetric holdup distributions in low volume fraction gas dispersions. However, much additional research is needed to come to a full understanding of these phenomena.

Acknowledgment

The authors wish to thank Lanre Oshinowo, Kumar Dhanasekharan, Elizabeth M. Marshall, Ahmad Haidari, and Sung-Eun Kim for their contributions.

REFERENCES

- Bakker A., Oshinowo L.M., Marshall E.M. (2000)
The Use of Large Eddy Simulation to Study Stirred Vessel Hydrodynamics. Proceedings of the 10th European Conference on Mixing, Delft, The Netherlands, July 2-5, 2000, page 247-254.
- Bakker A., LaRoche R.D., Wang M.H., Calabrese R.V. (1997)
Sliding Mesh Simulation of Laminar Flow in Stirred Reactors. TransIChemE, Vol. 75, Part A, page 42-44, January 1997.
- Bakker A., Van den Akker H.E.A. (1994a)
Single-Phase Flow in Stirred Reactors. Chemical Engineering Research and Design, TransIChemE, Vol. 72, Number A4, July 1994, page 583-593.
- Bakker A., Van den Akker H.E.A. (1994b)
Gas-Liquid Contacting with Axial Flow Impellers. Chemical Engineering Research and Design, TransIChemE, Vol. 72, Number A4, July 1994, page 573-582.
- Derksen, J., Van den Akker, H.E.A. (1999)
Large Eddy Simulations on the Flow Driven by a Rushton Turbine. AIChEJ, Vol. 45, No. 2, page 209-221.
- Eggels, J.G.M. (1996)
Direct and Large-Eddy Simulations of Turbulent Fluid Flow Using the Lattice-Boltzmann Scheme. Int. J. Heat Fluid Flow, Vol. 17, page 307.
- Lilly, D. K. (1966)
On the Application of the Eddy Viscosity Concept in the Inertial Subrange of Turbulence. NCAR Manuscript 123.
- Mathur (1994)
Unsteady Flow Simulations Using Unstructured Sliding Meshes. AIAA 25th Fluid Dynamics Conference, June 20-23, 1994, Colorado Springs, CO.
- Magelli F., and Montante G. (2002)

Personal communication.

Murthy, J. Y., and S. R. Mathur (1998)

A Finite Volume Method for Radiative Heat Transfer Using Unstructured Meshes. AIAA-98-0860, January, 1998.

Myers K.J., Ward R.W., Bakker A. (1997)

A Digital Particle Image Velocimetry Investigation of Flow Field Instabilities of Axial Flow Impellers. Journal of Fluids Engineering, Transactions of the ASME, Vol. 119, No. 3, page 623-632, September 1997.

Smagorinsky, J. (1963)

General Circulation Experiments with the Primitive Equations, I. The Basic Experiment. Month. Wea. Rev., Vol. 91, page 99 – 164.

Yakhot, A., S. A. Orszag, V. Yakhot, and M. Israeli (1986)

Renormalization Group Formulation of Large-Eddy Simulation. Journal of Scientific Computing, Vol. 1, page 1–51.